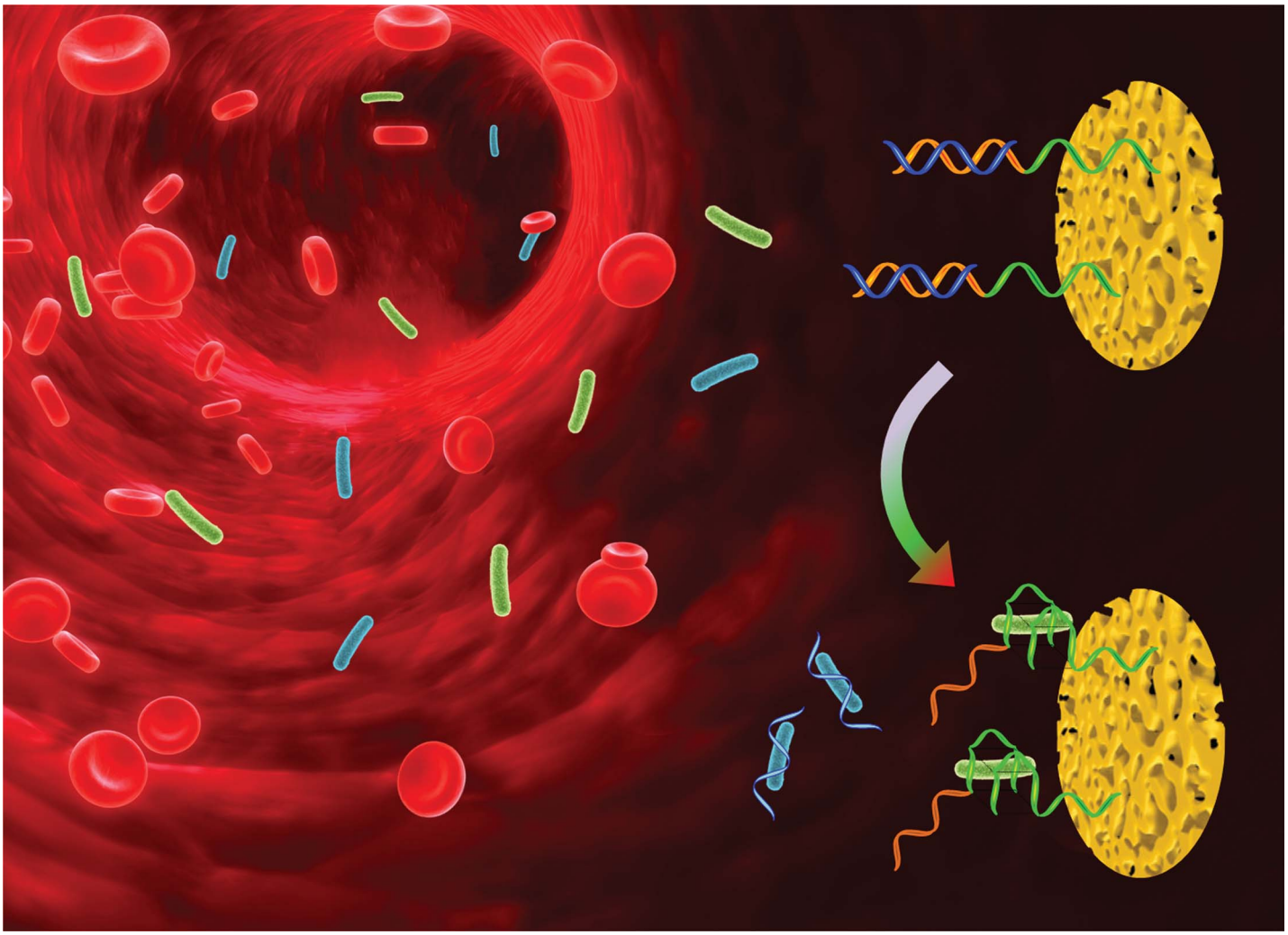

**Showcasing research from Prof. Wanqin Jin's group, State Key Laboratory of Materials-Oriented Chemical Engineering, College of Chemistry and Chemical Engineering, Nanjing University of Technology, P. R. China.**

Title: Three-dimensional porous microarray of gold modified electrode for ultrasensitive and simultaneous assay of various cancer biomarkers

A three-dimensional porous microarray of gold-modified electrode (PMGE) with a large surface area was successfully fabricated in this work. Based on the proposed PMGE, an aptasensor with excellent performance was designed and constructed for realizing the simultaneous assay of cancer biomarkers of angiogenin and thrombin.

## As featured in:

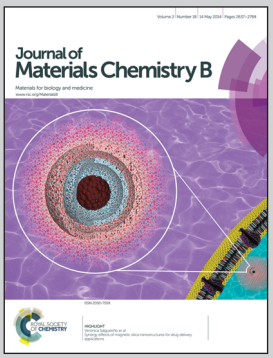


See Wanqin Jin *et al.*, *J. Mater. Chem. B*, 2014, **2**, 2658.

ROYAL SOCIETY OF CHEMISTRY

www.rsc.org/MaterialsB

Registered charity number: 207890

Journal of Materials Chemistry B

PAPER

View Article Online
View Journal | View Issue



Cite this: J. Mater. Chem. B, 2014, 2, 2658

# Three-dimensional porous microarray of gold modified electrode for ultrasensitive and simultaneous assay of various cancer biomarkers†

Lei Shi, Zhenyu Chu, Yu Liu, Jingmeng Peng and Wanqin Jin*

Received 3rd January 2014
Accepted 10th February 2014

DOI: 10.1039/c4tb00016a

www.rsc.org/MaterialsB

A three-dimensional (3D) microarray of a gold modified electrode with a nanoporous surface was successfully fabricated in this work. The special gold micro/nanostructure possessed an extremely high surface area (*ca.* 20 times its geometrical area), as well as highly stable and easily chemically modified properties, which could distinctly increase the binding sites for biological probes, facilitate the diffusion profile and enhance the electron transfer. Owing to these advantages, an ultrasensitive biosensor was designed on the porous microarray of the gold modified electrode (PMGE), which realized the simultaneous assay of cancer biomarkers of angiogenin (Ang) and thrombin (Tob). Under optimal experimental conditions, an impressively ultralow detection limit of 0.07 pM for Ang (a linear range from 0.2 pM to 10 nM) and a limit of 20 fM for Tob (a linear range from 50 fM to 5 nM) were obtained. Besides, the fabricated biosensor showed an excellent stability, good reproducibility and a high selectivity towards other biological proteins, which also exhibited promising potential for the application in a real serum sample analysis. Such a micro/nanostructure of gold could have widespread applications in biological sensing and quantitative biochemical analysis.

## Introduction

Aptamer biosensors (aptasensors), a special category of DNA biosensors, have received enormous interest, on account of their distinctive properties of high affinity and specificity toward extensive targets, *e.g.* small molecules, biological proteins and cells.[1–4] Generally, the construction of various aptasensors has mainly been based on fluorescence, colorimetric and electrochemistry techniques.[5–11] Among these methods, the electrochemical method is considered as one of the most attractive techniques for the simplicity, low cost, portability, and easy miniaturization. However, most of the known electrochemical aptasensors are restricted to the assay of a single analyte. Actually, in many advanced and practical applications, the simultaneous assays of multiplex analytes are encouraged and expected, because they can shorten the analytical time and decrease the detection cost.[12,13] Accordingly, the developing of multifunctional aptasensors with high performance are desired for measuring a large panel of disease markers present at ultralow levels during the early stages of disease progress. Recently, many efforts have been dedicated to the development of the simultaneous assay of different analytes. In these researches, two strategies were usually adopted in the sensing scheme. Firstly, various aptamer probes were adopted, to capture the corresponding targets respectively, in which the "signal on" sensing mechanism was achieved to acquire the enormous signal gain.[14–16] Secondly, a dual-functional probe consisting of different aptamer sequences was introduced.[17] In this condition, the adoption of a single aptamer probe effectively simplified the immobilization procedure and especially, made the fabricated aptasensor more reproducible. However, the introduction of different aptamer probes made the immobilization procedure complex and may not ensure the reproducibility of the assay results,[17] while the "signal-off" related architecture of the dual-functional probe limited the signal gains.[18] Therefore, it has remained a challenge to develop facile and sensitive assay strategies for the simultaneous assay of multiplex analytes.

In addition to a promising sensing scheme, the development and selection of new electrode materials is also considered a critical strategy to construct an excellent aptasensor.[13,15,16] Various micro/nanostructures based gold materials have been widely used in the construction of chemical and biological sensors, due to their unique physical and chemical properties, large surface area and easy chemical modification.[19–24] Among the multitudinous gold micro/nanostructures, three-dimensional

*State Key Laboratory of Materials-Oriented Chemical Engineering, College of Chemistry and Chemical Engineering, Nanjing University of Technology, Nanjing 210009, P. R. China. E-mail: wqjin@njut.edu.cn; Fax: +86-25-8317-2292; Tel: +86-25-8317-2266*

† Electronic Supplementary Information (ESI) available: Characterization of gold structures electrodeposited with different charge (Fig. S1); Adsorption/desorption isotherms of PMGE (Fig. S2); Signal responses of the Rp-A (Fig. S3); Assay of Ang and Tob based on bare gold slice (Fig. S4); Reproducibility and stability tests (Fig. S5); Performance comparisons of different aptasensors (Table S1); Assay results in human serum sample (Table S2). See DOI: 10.1039/c4tb00016a

(3D) structures, *e.g.* the ordered macroporous gold film,[25,26] gold nanowires,[27,28] and fractal gold micro/nanostructure,[29] have attracted special interest in electrochemical biological assays. In these sensing systems, the 3D micro/nanostructures enhanced the acquisition and transmission of the signals and finally, contributed to the increased performance, which was mainly due to the large surface area of the 3D structures increasing the binding sites for the probe molecules, providing more reaction positions for interfacial reactions and making the biomolecule easily accessible to the electrode surface. Therefore, it is highly inspired and deserved to fabricate novel 3D gold micro/nanostructures with a significantly enlarged surface area for constructing sensitive biosensors.

In this work, we present a novel 3D porous microarray of a gold modified electrode (PMGE), which was suitable for constructing ultrasensitive aptasensors. The proposed porous microarray of gold was successfully prepared, based on an inorganic–organic hybrid template. The 3D PMGE possessed an extremely large surface area, which could significantly increase the binding sites for biological probes and thence, improve the performance. Here, two important analytes, angiogenin (Ang) and thrombin (Tob) were selected as samples, to demonstrate the superior ability of the PMGE in sensing applications, because these two analytes are closely related to the activation and proliferation of cancer cells and the corresponding concentrations of the analytes would increase obviously in the serum.[30–33] Accordingly, an aptasensor was designed for the simultaneous assay of cancer biomarkers of Ang and Tob, based on the PMGE for the first time, in which a "signal on" sensing scheme was realized by introducing a single capture probe. The constructed aptasensor showed an excellent performance in the assay of Ang and Tob, which also presented a fascinating application in a real serum sample. It was confirmed that a reliable and constructive aptasensor was developed on the 3D PMGE.

# Experimental section

### Chemicals and materials

Gold(III) chloride trihydrate ($HAuCl_4$, 99.99%) was obtained from Alfa Aesar, gold nanoparticles (AuNPs) with a 10 nm diameter were purchased from Strem Chemicals. Thrombin (Tob), angiogenin (Ang), lysozyme (Lzm), bovine serum albumin (BSA), hemoglobin (Hb), immunoglobulin G (IgG), 6-mercapto-1-hexanol (MCH), Tri(2-carboxyethyl) phosphine hydrochloride (TCEP, 98%), Hexaammineruthenium(III) chloride (RuHex), and tris(hydroxymethyl)aminomethane (Tris–base) were obtained from Sigma-Aldrich. All the oligonucleotides were synthesized by TaKaRa Biotechnology Co., Ltd. (Dalian, China), and their base sequences were as follows: capture probe: 5′–SH–$(CH_2)_6$–AGT CCG TGG TAG GGC AGG TTG GGG TGA CT TGA GAA TGA ACG CTG GAT CCA-3′, the sequence of "AGT CCG TGG TAG GGC AGG TTG GGG TGA CT" represented the aptamer for Tob (Apt-T), and the sequence "TGA GAA TGA ACG CTG GAT CCA" was partially complemented with the aptamer for Ang (Apt-A). Apt-A: 5′-CGG ACG AAT GCT TTG ATG TTG TGC TGG ATC CAG CGT TCA TTC TCA-3′, reporter probes of Ang (Rp-A): 5′–SH–TGG ATC CAG CGT-3′ (Rp-A I) and 5′–SH–GGG AAA AAA GGG–MB-3′ (Rp-A II), reporter probes of Tob (Rp-T): 5′–SH–GGT TGG TGT GGT TGG-3′ (Rp-T I, another aptamer for binding with the fibrin exosite on Tob)[34] and 5′–SH–GGG AAA AAA GGG–Fc-3′ (Rp-T II). Here, the sequences of Rp-A I and Rp-T I were adopted to bind with the capture probe and Tob respectively, and the Rp-A II and Rp-T II were served as the electrochemical indicators in the assay of Ang and Tob respectively, on account of the MB and Fc in the sequences. The other chemicals employed were all of analytical grade and triple distilled water was used throughout.

### Fabrication of the 3D PMGE

A highly oriented hybrid microarray, prepared in previous work, was used as the template for the preparation of a porous gold microarray.[35,36] The amperometric *i–t* curve technique was employed for the electrochemical deposition, the electrolyte contained 5 mM of $HAuCl_4$ and a potential of 0.5 V was adopted here. A different deposition time was applied to investigate the effect of the deposition charge on the morphologies of the fabricated gold structures. After the electrodeposition, the modified electrode was dipped into 0.1 M $HNO_3$ to sufficiently remove the hybrid template and the 3D PMGE was subsequently obtained. Then, the PMGE was cycled in a 0.5 M $H_2SO_4$ aqueous solution to remove any residual impurities. Finally, the freshly cleaned PMGE was dried with nitrogen gas and served for the immobilization of the capture probes.

### Material characterization

The morphologies of the PMGE were observed by field-emission scanning electron microscopy (FESEM, Hitachi S4800), and the chemical composition of the PMGE was determined by energy-dispersive X-ray spectroscopy (EDX, Hitachi S4800). The analysis of the X-ray photoelectron spectra (XPS) was performed on an ESCLAB MKII. The X-ray diffraction (XRD) was measured on an X-ray diffractometer (D/MAX 2500 V/PC) with a Cu-Ka line (0.15419 nm). The structure parameters of the PMGE were investigated by the $N_2$ adsorption–desorption isotherms, which were performed using an automated surface area analyzer (Beckman Coulter SA-3100 Gas Adsorption Surface Area and Pore Size Analyzer). A sample of 0.20 g was first outgassed at 50 °C, for 60 min, under a vacuum and then the isotherm was measured over the relative pressure ($P/P_0$) ranging from 0.01 to 0.99 and back. The BET specific surface area ($S_{BET}$) was determined using the Brunauer–Emmett–Teller (BET) equation. The specific surface area of the PMGE was calculated from the BET, and the pore volume was assessed. The pore volume *versus* the diameter distribution was calculated by analyzing the adsorption branch of the isotherm using the Barrett–Joyner–Halenda (BJH) method.[37,38]

### Functionalization of AuNPs with Rp-T and Rp-A

The reporter probe–AuNP conjugates were introduced to amplify the response signals, which were prepared with the following procedure.[39] The AuNPs were firstly added to the Rp-T and Rp-A in sterilized water and incubated at 4 °C, for 16 h. The concentration of Rp-T I and Rp-A I was 0.1 μM, while the concentration of Rp-T II and Rp-A II was 1 μM. Then, reporter

probe–AuNPs conjugates were aged by gradually adding 2 M NaCl every 30 min, to reach a final salt concentration of 0.1 M NaCl. The mixed solution was incubated for 48 h and finally the solution was centrifuged for 30 min at 4 °C, with the supernatant being removed. The red oily precipitate was washed with 10 mM phosphate buffered solution (PBS, pH 7.4), recentrifuged, and then redispersed in 10 mM PBS buffer.

### Construction of the 3D PMGE based aptasensor for simultaneous assay of Ang and Tob

The freshly cleaned PMGE was immersed in an immobilization buffer of 10 mM Tris–HCl, 1 mM EDTA, 10 mM TCEP, and 0.1 M NaCl at pH 7.4 containing 2 μM of the capture probe for 5 h. After the unbound probes were washed away with a washing buffer (10 mM Tris–HCl, pH 7.4), the unreacted active surface groups were subsequently passivated by reaction with a 500 nM MCH solution for 4 h. Then, it was immersed in 10 mM PBS (pH 7.4) with 0.25 M NaCl, containing 5 μM Apt-A for 2 h. After the hybridization, the PMGE was extensively rinsed with washing buffer. Subsequently, the sensing interface was immersed in a mixture of Ang and Tob with various concentrations for 4 h, again followed by thoroughly washed with the washing buffer. Afterwards, AuNPs labeled Rp-T and Rp-A was added to the detection system for 6 h at 37 °C.

### Quantitative assay of Ang and Tob in human serum

Healthy human serum was used to confirm the applicability of this aptasensor. The serum sample was loaded into a centrifugal filter device, and subjected to centrifugation (12 000*g*, 15 min).[31] The serum centrifugation ultrafiltrate was used for the following measurements. The concentrations of Ang and Tob in the blank serum sample were firstly detected by the obtained calibration plots of the fabricated aptasensor, and the background signals would be deducted in the subsequent quantitative assay. Then, different concentrations of standard solutions of Ang and Tob were added to the 100 times diluted serum and the electrochemical assay was performed.

### Electrochemical measurements

All the electrochemical measurements were performed with a CHI 660C electrochemical workstation (Shanghai Chenhua, China). The three-electrode system used consisting of the 3D PMGE working electrode, a platinum auxiliary electrode, and an Ag/AgCl (saturated KCl) reference electrode. Cyclic voltammetry (CV) was carried out at different scan rates, square wave voltammetric (SWV) measurements were taken at a frequency of 5 Hz, electrochemical impedance spectroscopy (EIS) measurements were performed with the frequency changed from 0.01 Hz to 100 kHz with a signal amplitude of 5 mV and chronocoulometry (CC) measurements were conducted at a pulse width of 0.25 s. The electrolytes for CV and SWV was 10 mM PBS and 0.25 M NaCl (pH 7.4), for CC was 10 mM Tris–HCl (pH 7.4) and for EIS was 5 mM $K_3[Fe(CN)_6]$/$K_4[Fe(CN)_6]$ and 0.1 M KCl solution. During the CC measurement, a nitrogen atmosphere was maintained to avoid air sliding into the electrochemical cell.

## Results and discussion

### Characterizations of the 3D PMGE

A gold microarray with a porous structure on the surface was successfully fabricated, as shown in Fig. 1. Compared with the hybrid template consisting of the hexagonal prism-shaped crystals with an average side length of *ca.* 5 μm (Fig. 1A), the maintained morphology of the microarray with an enlarged dimension of gold hexagonal prisms was produced when an appropriate electrodeposition charge of 0.6 C was implemented, shown in Fig. 1B. It can be seen that gold nanoparticles were consecutively formed and ranged along the outside surface of the template, and the gold prism with a side length of *ca.* 7 μm was prepared (Fig. 1C). Especially, with a high magnification focused on the surface of the obtained gold prism, a porous structure was created in this condition (Fig. 1D), which could further improve the surface area of the PMGE. In addition, the effect of the deposition charge on the morphologies of the obtained gold micro/nanostructures was investigated. It was found that less or more charge would not create the desired PMGE with a large surface area. If a lower charge of 0.2 C was adopted, the formed gold particles would not completely cover the surface of the hybrid template, leading to the collapse of the array, once the template was removed. When a charge of 1.2 C was implemented, more gold was reduced and the partial gold particles would be prone to fill the interspaces among each array of the PMGE, which inversely decreased its surface area, as shown in Fig. S1 in the ESI.†

As the purity, stability and chemical modification properties of the fabricated gold structure play a critical role in its biosensing applications, therefore EDX, XRD and XPS characterizations were carried out to analyze the elemental composition and explore the surface property of the PMGE. As shown in Fig. 2A, it was demonstrated that the hybrid template was sufficiently removed after the modified electrode was treated with the $HNO_3$ solution, and the gold element became the

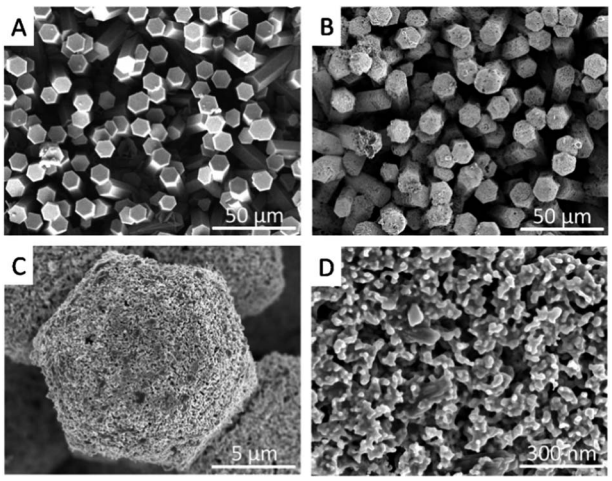


Fig. 1 FESEM images of (A) the template of hybrid microarray, (B) the fabricated 3D PMGE, (C) the gold hexagonal prism, (D) nanoporous structure on the surface of the gold prism.

 

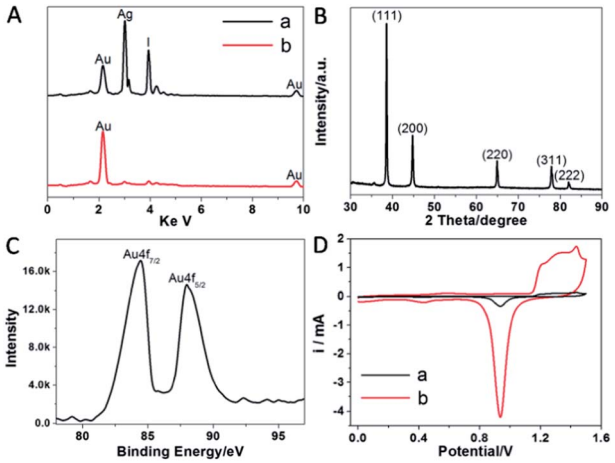


Fig. 2 (A) EDX images of the 3D PMGE (a) before (b) after the treatment with 0.1 M $HNO_3$, (B) and (C) XRD pattern and XPS spectrum of the 3D PMGE. (D) Cyclic voltammograms in 0.1 M $H_2SO_4$ solution, (a) bare electrode, (b) the 3D PMGE.

dominating component of the obtained PMGE. The XRD pattern for the PMGE is shown in Fig. 2B, and it is obvious that the characteristic peaks belong to fcc Au. The peaks located at 38.0, 44.2, 64.5, 77.5 and 81.7° were assigned to the (111), (200), (220), (311) and (222) facets, respectively. Especially, the intensity ratio (2.6) of the {111} to the {200} diffraction line was higher than that of the standard diffraction of gold powder (1.9), indicating that the deposited porous gold structure had a tendency to grow with the surfaces dominated by the lowest energy {111} facets.[40] Moreover, the gold $4f_{7/2}$ and $4f_{5/2}$ doublet with the binding energies of 84.2 and 87.9 eV in the XPS spectrum implied the gold valence state was $Au^0$ (shown in Fig. 2C),[41] which was essential for the interaction with thiolated probes through the Au–S bond. The results of the EDX, XRD and XPS analyses confirmed that the PMGE possessed a pure component, high stability and easily chemically modified properties.

Furthermore, as shown in the adsorption–desorption isotherms in Fig. S2 in the ESI,† the isotherms of the PMGE showed a class IV behavior. The steep increase in the isotherm slope at high $P/P_0$, above 0.95, may be due to the capillary condensation within the pores, followed by saturation as the pores become filled with liquid.[37,38] Due to the pore size ranging from the mesopore to a low macropore (shown in Fig. 1D), the capillary condensation and steep rise in the isotherm occurs at relatively high values of $P/P_0$, as expected on the basis of the Kelvin equation. In addition, the analysis of the adsorption branch was introduced to assess the pore size distribution of the PMGE, which was considered as a more realistic method for this kind of sample. The $S_{BET}$ of the PMGE was estimated to be *ca.* 6.7 $m^2\ g^{-1}$, which is higher than that of some reported nanoporous gold structures,[38] and a pore size of 58 nm, with a pore volume of 0.052 $cm^3\ g^{-1}$ were obtained. In addition, the roughness factor ($R_f$) of the PMGE was electrochemically investigated in 0.1 M $H_2SO_4$, at a scan rate of 100 mV $s^{-1}$,[26] which is shown in Fig. 2D. Gold oxidation started at about 1.2 V, showing three anodic current peaks. The formed gold oxide was then electrochemically reduced in the negative potential sweep. By integrating the charge required for reducing the gold oxide formed in the positive sweep, the real surface area of the PMGE was determined to be 2.40 $cm^2$. Assuming that the reduction of a monolayer of gold oxide requires 386 $\mu C\ cm^{-2}$, whereas the geometrical area of the bare gold electrode was only 0.12 $cm^2$, the $R_f$ of the PMGE was calculated to be *ca.* 20, which was attributed to the micro/nanostructure of the 3D array and porous surface.

All of these promising properties, *e.g.* a significantly enhanced surface area, pure component, high stability and easy chemical modification, would make the fabricated PMGE a good candidate for the construction of ultrasensitive aptasensors.

## Design of the 3D PMGE based multiplex analytes sensing scheme

Compared with previously reported work, an improved sensing scheme was conceived by introducing the "signal on" strategy based on the single capture probe in this work. The construction scheme of the developed aptasensor is shown in Fig. 3. The 5′-thiolated capture probe consisting of the Apt-T sequence and a complementary sequence of Apt-A was firstly immobilized on the PMGE through the Au–S bond. Then, the Apt-A was introduced to partially hybridize with the capture probe, which was critical for realizing the "signal on" sensing strategy. Since the aptamer could bind tightly and specifically to its target molecule to form a tertiary complex with a binding constant greater than that of an ordinary DNA duplex, therefore, once the analytes of Ang and Tob were added into the detection system, the Apt-A and Apt-T would bind with Ang and Tob, respectively and fold to the complex structures. As a result, a complex structure of a Tob-aptamer was confined at the surface of the PMGE while

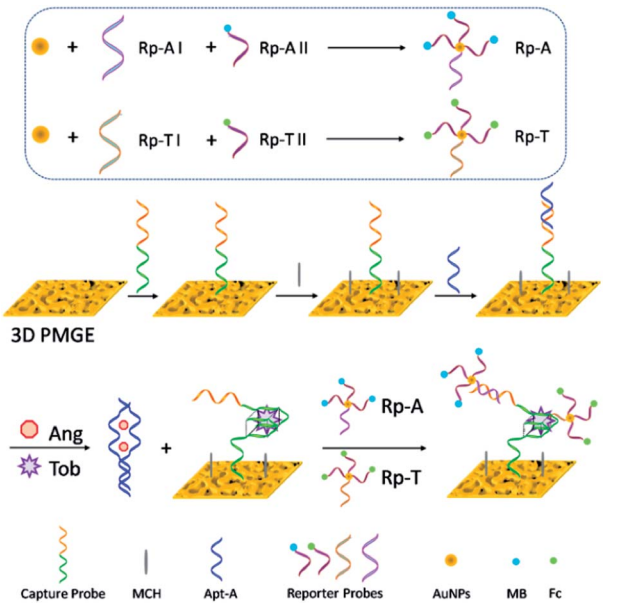


Fig. 3 Schematic illustration of the 3D PMGE based electrochemical aptasensor for the simultaneous assay of Ang and Tob.

another complex of an Ang–aptamer was disassociated from the electrode surface, leading to the formation and exposure of binding sites for the reporter probes. Finally, the Rp-A and Rp-T were added to the detection system, which could bind with the complementary sequence of Apt-A and Tob respectively, realizing the "signal on" sensing strategy.

### Electrochemical characterization of the aptasensor

EIS could give information on the resistance of interfacial electron transfer, which was implemented to monitor the impedance changes during the different sensing interfaces.[26,36,42] The impedance spectra included a semicircle portion and a linear portion. The semicircle portion at higher frequencies corresponded to the electron-transfer limited process, and the linear portion, at lower frequencies, represented the diffusion-limited process. The semicircle diameter equalled the electron-transfer resistance, $R_{et}$. As shown in Fig. 4A, the PMGE possessed an extremely small semicircle (curve *a*), implying a low resistance to the redox indicator of $[Fe(CN)_6]^{3-/4-}$ in solution, which was attributed to the larger electroactive surface and higher conductivity of the PMGE. When the capture probe was immobilized onto the PMGE, the resistance increased apparently (curve *b*), mainly due to the electrostatic repulsion from the negatively charged phosphate backbone of the oligonucleotide strands. Subsequently, after the passivation reaction of MCH and hybridization with Apt-A, the steric hindrance and electrostatic repulsion became larger, resulting in a high electron-transfer resistance of the redox probe (curve *c* and curve *d*). Once the analytes of Tob and Ang were injected, the formed complex of Ang–aptamer was disassociated from the electrode surface, while the Tob–aptamer complex was fixed on the electrode surface. At this moment, the steric hindrance of the Tob–aptamer complex played a primary role on the interfacial electron transfer, therefore the semicircle further increased (curve *e*). After the indicators Rp-A and Rp-T were introduced to the detection system, the significantly improved steric hindrance and electrostatic repulsion were formed in the sensing interface, resulting in a remarkably increased resistance (curve *f*).

Meanwhile, CV was introduced to monitor the current response (*i*) in the assay. When the Ang and Tob were simultaneously added, two separated pairs of signal responses were observed (curve a in Fig. 4B), which were due to the redox of MB and Fc, respectively, indicating that the designed sensing strategy was feasible in the assay of Ang and Tob. In contrast, in the absence of the analytes, only a smooth cyclic curve was observed, which is shown in curve *b* of Fig. 4B. Furthermore, the cross-reactivity between the different analytes of the as-fabricated aptasensor was evaluated by comparing the signal responses obtained in the presence of both Ang and Tob to the electrochemical signals obtained with only one analyte present. As shown in Fig. 4C, when the Ang was added to the detection system, a redox pair of MB was obtained in the CV curve (curve *b*). However, a lower peak current, with a larger peak separation, was observed compared with that in the presence of Ang and Tob simultaneously. This may be due to that the formation of the complex of Tob–aptamer shortened the distance of the Rp-A to the PMGE surface,[43,44] which facilitated the electron transfer of the MB to the electrode. While in the presence of Tob, a redox pair of Fc was obtained in the CV curve, with no obvious change in the signal response (Fig. 4D). The results definitely indicated that the simultaneous assay of the Ang and Tob not only showed minimal interference with each other, but excavated the potential of the fabricated aptasensor, in which an improved performance could be obtained, compared to that when only one analyte was present.

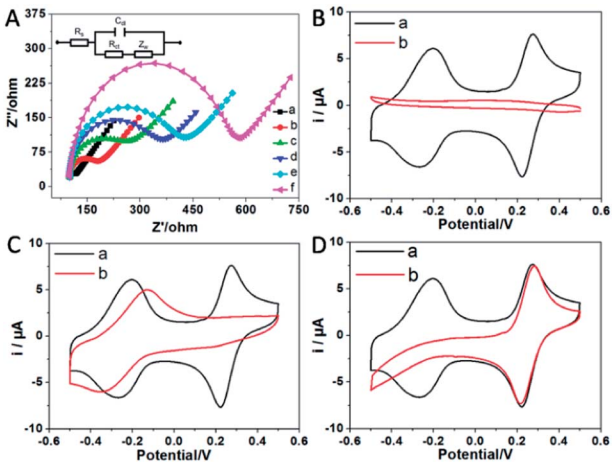


Fig. 4 (A) Nyquist plots in the $Fe(CN)_6^{3-/4-}$ solution of the aptasensor at different sensing interfaces. (a) the PMGE, (b) capture probe immobilized PMGE, (c) after the passivation with MCH, (d) after the hybridization of Apt-A, (e) after the injection of Ang and Tob, (f) after the addition of Rp-T and Rp-A. (B) CVs in the PBS solution. (a) in the presence of 0.1 nM Ang and 50 pM Tob, (b) in the absence of the analytes. (C) CVs in the PBS solution. (a) in the presence of 0.1 nM Ang and 50 pM Tob, (b) in the presence of 0.1 nM Ang. (D) CVs in the PBS solution. (a) in the presence of 0.1 nM Ang and 50 pM Tob, (b) in the presence of 50 pM Tob.

### Optimization of experimental conditions on the signal responses

On account of the introduction of a single capture probe in this work, the optimized probe density was readily realized by incubating the 2 μM probe for various amounts of time. CC was introduced to investigate the probe density on the PMGE, and RuHex served as the electrochemical indicator in the CC experiments, which was stoichiometrically bound to the anionic phosphodiester backbone of the oligonucleotide and therefore quantitatively reflected the amount of oligonucleotide strands on the surface.[45] As shown in Fig. 5A, with the incubation time ranging from 1 to 9 h, the value of the probe density increased from $1.1 \times 10^{11}$ to $5.6 \times 10^{12}$ molecules $cm^{-2}$. While further increasing the incubation time to 13 h, no obvious increment in the density was observed. Meanwhile, more attention was focused on whether the resulting density could lead to the good electrochemical signal responses. Consequently, the performance of the fabricated aptasensor based on various probe densities was investigated. As shown in Fig. 5B, the higher current signals (i) of both Ang and Tob were observed with a

 

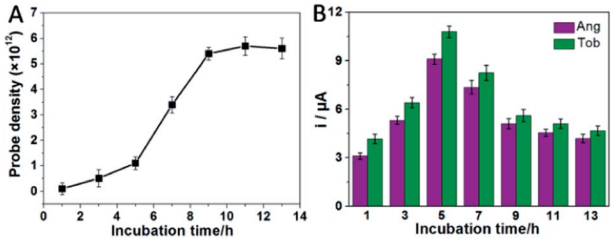


Fig. 5 (A) Probe density on the surface of PMGE incubated with 2 μM capture probe for 1 h, 3 h, 5 h, 7 h, 9 h, 11 h and 13 h respectively. (B) Effect of the probe density on the signal responses of Ang and Tob respectively. Five independent experiments were implemented in each measurement.

proper incubation time of 5 h, in which the probe density was estimated to be *ca.* $1.3 \times 10^{12}$ molecules $cm^{-2}$. As we know, the lower probe density usually led to the generation of weak signals, while a higher density resulted in an increased steric hindrance, which severely hindered the interactions between the oligonucleotide strands and biological proteins.[46]

In addition, it was crucial to make all of the capture probes possibly hybridized with the Apt-A, which was significantly pivotal to obtain a large signal change before/after the addition of analytes to achieve the excellent performance. Therefore, after the Apt-A was hybridized with capture probe for different times ranging from 0.5 to 4 h, the reporter of Rp-A was added to the assay system and the corresponding signal responses were recorded. As shown in Fig. S3 in the ESI,† with the increased time of incubation, more capture probes were hybridized with the Apt-A and a reduction in the signal responses of the MB was observed. When an incubation time over 2 h was introduced, the signal response of the Rp-A approached a minimum level, indicating that in this condition nearly all of the capture probes were successfully hybridized with the Apt-A. As a result, an incubation time of 2 h was provided to ensure a thorough hybridization between the capture probe and Apt-A.

## Performance of the fabricated aptasensor

The sensitivity of the electrochemical aptasensor was investigated by varying the concentrations of the Tob and Ang, and the SWV was implemented to monitor the current change ($\Delta i$, the changes of peak current before/after the addition of analytes). As shown in Fig. 6A, the current signals (i) for the simultaneous detection of Ang and Tob increased with the increment of Ang and Tob concentrations in the sample solution. The calibration plots showed a good linear relationship between the peak current changes and the concentrations of analytes (Fig. 6B), and regression equations of $\Delta i = 20.53 + 1.53 \log C_{Ang}$ ($R^2 = 0.997$) and $\Delta i = 25.31 + 1.77 \log C_{Tob}$ ($R^2 = 0.998$) were obtained in Ang and Tob, respectively. Based on the developed aptasensor, ultrasensitive and simultaneous assay of Ang and Tob was realized. An ultralow detection limit of 0.07 pM for Ang with a linear range from 0.2 pM to 10 nM and a detection limit of 20 fM for Tob with a linear range from 50 fM to 5 nM were achieved respectively ($S/N = 3$). The detectable concentrations of Ang and Tob in the present work were even comparable to the detection

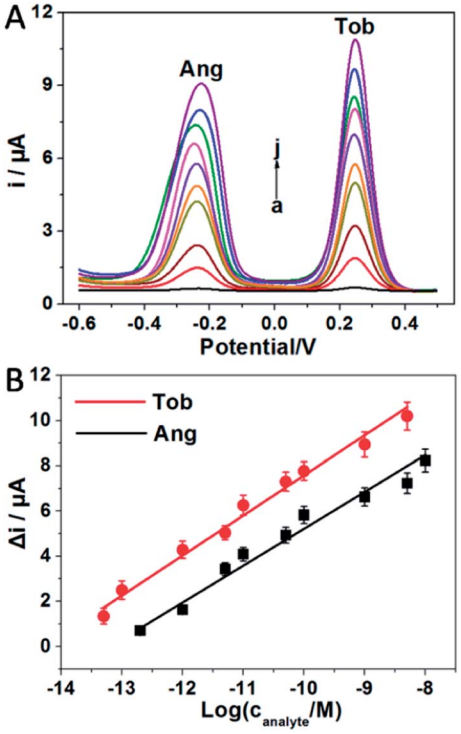


Fig. 6 (A) SWV responses of the proposed aptasensor after incubation with Ang and Tob of different concentrations (Ang, from curve a to j: 0 pM, 0.2 pM, 1 pM, 5 pM, 10 pM, 50 pM, 0.1 nM, 1 nM, 5 nM and 10 nM; Tob, from curve a to j: 0 fM, 50 fM, 0.1 pM, 1 pM, 5 pM, 10 pM, 50 pM, 0.1 nM, 1 nM and 5 nM). (B) Calibration curves for the simultaneous assay of Ang and Tob (five independent experiments were implemented here).

limits reported in some single analyte aptasensors (typically 1 pM to 1 nM for Ang and 0.1 pM to 6.4 nM for Tob, shown in Table S1 in the ESI†).[5,28,31,47–50] In addition, similar assay of Ang and Tob based on the bare gold slice was also investigated. Under the same conditions as during the assay, higher detection limits of 0.5 nM and 30 pM were observed in the detection of Ang and Tob, respectively (Fig. S4 in the ESI†). It should be noted that the sensitivity of the 3D PMGE based aptasensor was almost 3 orders of magnitude higher than that based on the bare gold slice, confirming that the significantly enhanced surface area, as well as the high stability of the 3D PMGE plays a critical role in the ultrasensitive assay.

## The specificity, reproducibility and stability of the aptasensor

In addition to the sensitivity of an aptasensor, the specificity, reproducibility and stability of aptasensor were also extremely important for the practical applications. The specificity of the aptasensor was determined by challenging it with 1 mM Lzm, 1 mM Hb, 1 mM BSA, 1 mM IgG and a mixture of them, respectively. As shown in Fig. 7, the aptasensor showed an almost negligible response to other proteins, or a mixture, compared with that of 5 pM Tob and 10 pM Ang. The results indicated that the aptasensor possessed excellent selectivity for Tob and Ang, over other the biological proteins, attributed to the highly

specific interactions between the aptamers and the related proteins.

In order to inspect the reproducibility of the aptasensor, five freshly prepared modified electrodes were incubated with a mixture of 10 pM Ang and 5 pM Tob. All five electrodes exhibited a similar amperometric response behavior, and the relative standard deviations (RSD) were 4.2% and 5.0% for Ang and Tob, respectively (Fig. S5A in the ESI†). This demonstrated that the reproducibility of the proposed aptasensor for Ang and Tob was acceptable, which was due to the good stability of the 3D PMGE and the introduction of the single capture probe.

Furthermore, the probe modified electrode was firstly stored in a refrigerator at 4 °C for 1 week, 2 weeks and 3 weeks, respectively, and then examined after adding the analytes and reporter probes. Based on the perfect stability of the 3D PMGE, the results of the experiments showed that the aptasensor retained about 87% and 91% of its initial responses of Ang and Tob, respectively, even after 3 weeks (Fig. S5B in the ESI†), indicating an excellent stability of the fabricated aptasensor.

### Practical applications of the aptasensor

Owing to the excellent sensitivity and selectivity of our proposed aptasensor, here we assessed the performance of this aptasensor to detect the Ang and Tob in real human serum. The blank human serum was firstly detected according to the obtained calibration plots, and no Tob and 5 nM Ang (RSD = 4.1%) were found in the blank serum sample. The standard addition method was then employed to evaluate the applicability of the aptasensor. The real serum was diluted 100 times before each trial, and the background signal was deducted in the quantitative assay. The analytical results for Ang and Tob are shown in Table S2 in the ESI.† From Table S2,† we could see that the recovery (between 95% and 101%) and RSD (between 2.7% and 3.9%) were satisfactory, which clearly indicated the aptasensor possessed a promising potential for the simultaneous detection of Ang and Tob in real biological samples.

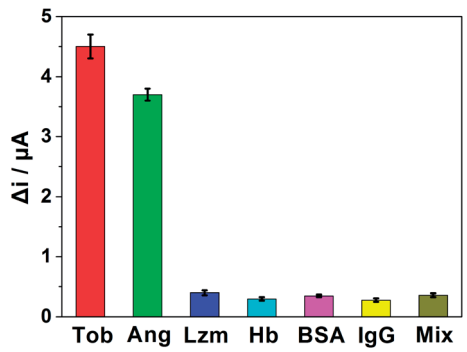


Fig. 7 Selectivity evaluation of the proposed aptasensor for 10 pM Ang and 5 pM Tob against 1 mM Lzm, 1 mM Hb, 1 mM BSA, 1 mM IgG and a mixture respectively, and five independent experiments were implemented.

## Conclusions

A 3D porous gold microarray based ultrasensitive electrochemical aptasensor was successfully constructed for the simultaneous assay of cancer biomarkers of Ang and Tob in this work. The porous microarray of a gold modified electrode with a significantly enhanced surface area, pure component, and high stability proved to be a promising candidate for constructing an ultrasensitive aptasensor. The proposed "signal on" sensing scheme based on the single capture probe simplified the immobilization procedure of the probe, effectively facilitated the acquisition of the response signals and ensured the reproducibility of the assay results. On account of these merits, the fabricated aptasensor showed ultrasensitive detection limits of Ang and Tob simultaneously, as well as excellent stability, good reproducibility and high selectivity towards other biological proteins. The fabricated aptasensor also showed a promising potential for the application in real serum sample analysis. It was believed that the proposed 3D PMGE could have great promise in constructing other sensitive and selective aptasensors for the clinical diagnosis of disease-related biomarkers.

## Acknowledgements

This work was supported by the Innovative Research Team Program by the Ministry of Education of China (no. IRT13070), the Doctoral Fund of Ministry of Education of China (20113221110001), the National Natural Science Foundation of China (no. 21176115), and the Innovation Foundation for Doctoral Dissertation of Jiangsu Province (CXLX12_0443).

## Notes and references

1 A. A. Lubin and K. W. Plaxco, *Acc. Chem. Res.*, 2010, **43**, 496–505.
2 I. Willner and M. Zayats, *Angew. Chem., Int. Ed.*, 2007, **46**, 6408–6418.
3 J. Liu, Z. Cao and Y. Lu, *Chem. Rev.*, 2009, **109**, 1948–1998.
4 W. Tan, M. J. Donovan and J. Jiang, *Chem. Rev.*, 2013, **113**, 2842–2862.
5 W. Li, K. Wang, W. Tan, C. Ma and X. Yang, *Analyst*, 2007, **132**, 107–113.
6 P. Hu, C. Zhu, L. Jin and S. Dong, *Biosens. Bioelectron.*, 2012, **34**, 83–87.
7 H. Huang, Y. Tan, J. Shi, G. Liang and J. J. Zhu, *Nanoscale*, 2010, **2**, 606–612.
8 J. W. Liu and Y. Lu, *Angew. Chem., Int. Ed.*, 2006, **45**, 90–94.
9 C. C. Chang, S. C. Wei, T. H. Wu, C. H. Lee and C. W. Lin, *Biosens. Bioelectron.*, 2013, **42**, 119–123.
10 Y. Peng, D. Zhang, Y. Li, H. Qi, Q. Gao and C. Zhang, *Biosens. Bioelectron.*, 2009, **25**, 94–99.
11 D. W. Zhang, C. J. Sun, F. T. Zhang, L. Xu, Y. L. Zhou and X. X. Zhang, *Biosens. Bioelectron.*, 2012, **31**, 363–368.
12 J. A. Hansen, J. Wang, A. N. Kawde, Y. Xiang, K. V. Gothelf and G. Collins, *J. Am. Chem. Soc.*, 2006, **128**, 2228–2229.
13 L. Bai, R. Yuan, Y. Chai, Y. Zhuo, Y. Yuan and Y. Wang, *Biomaterials*, 2012, **33**, 1090–1096.

 

14 Y. Du, B. Li, H. Wei, Y. Wang and E. Wang, *Anal. Chem.*, 2008, **80**, 5110–5117.
15 Y. Xiang, X. Qian, Y. Zhang, Y. Chen, Y. Chai and R. Yuan, *Biosens. Bioelectron.*, 2011, **26**, 3077–3080.
16 T. Zheng, T. Tan, Q. Zhang, J. J. Fu, J. J. Wu, K. Zhang, J. J. Zhu and H. Wang, *Nanoscale*, 2013, **5**, 10360–10368.
17 X. Li, J. Liu and S. Zhang, *Chem. Commun.*, 2010, **46**, 595–597.
18 Y. Xiao, B. D. Piorek, K. W. Plaxco and A. J. Heeger, *J. Am. Chem. Soc.*, 2005, **127**, 17990–17991.
19 K. Saha, S. S. Agasti, C. Kim, X. Li and V. M. Rotello, *Chem. Rev.*, 2012, **112**, 2739–2779.
20 Y. H. Tan, J. R. Schallom, N. V. Ganesh, K. Fujikawa, A. V. Demchenko and K. J. Stine, *Nanoscale*, 2011, **3**, 3395–3407.
21 Z. Chen, Y. Lei, H. Xu, X. Chen and J. Liu, *J. Mater. Chem. B*, 2013, **1**, 3031–3034.
22 Y. Pei, Z. Wang, S. Zong and Y. Cui, *J. Mater. Chem. B*, 2013, **1**, 3992–3998.
23 L. Shi, Z. Chu, Y. Liu, W. Jin and X. Chen, *Biosens. Bioelectron.*, 2013, **49**, 184–191.
24 K. M. Pondman, A. W. Maijenburg, F. B. Celikkol, A. A. Pathan, U. Kishore, B. ten Haken and J. E. ten Elshof, *J. Mater. Chem. B*, 2013, **1**, 6129–6136.
25 C. H. Wang, C. Yang, Y. Y. Song, W. Gao and X. H. Xia, *Adv. Funct. Mater.*, 2005, **15**, 1267–1275.
26 X. Chen, Y. Wang, J. Zhou, W. Yan, X. Li and J. J. Zhu, *Anal. Chem.*, 2008, **80**, 2133–2140.
27 R. Gasparac, B. J. Taft, M. A. Lapierre-Devlin, A. D. Lazareck, J. M. Xu and S. O. Kelley, *J. Am. Chem. Soc.*, 2004, **126**, 12270–12271.
28 Y. L. Chen, C. Y. Lee and H. T. Chiu, *J. Mater. Chem. B*, 2013, **1**, 186–193.
29 L. P. Xu, S. Wang, H. Dong, G. Liu, Y. Wen, S. Wang and X. Zhang, *Nanoscale*, 2012, **4**, 3786–3790.
30 N. Yoshioka, L. Wang, K. Kishimoto, T. Tsuji and G. F. Hu, *Proc. Natl. Acad. Sci. U. S. A.*, 2006, **103**, 14519–14524.
31 W. Li, X. Yang, K. Wang, W. Tan, H. Li and C. Ma, *Talanta*, 2008, **75**, 770–774.
32 W. Ruf and B. M. Mueller, *Semin. Thromb. Hemostasis*, 2006, **32**, 61–68.
33 M. Franchini and P. M. Mannucci, *Semin. Thromb. Hemostasis*, 2012, **38**, 95–101.
34 L. C. Bock, L. C. Griffin, J. A. Latham, E. H. Vermaas and J. J. Toole, *Nature*, 1992, **355**, 564–566.
35 L. Shi, Z. Chu, X. Dong, W. Jin and E. Dempsey, *Nanoscale*, 2013, **5**, 10219–10225.
36 L. Shi, Z. Chu, Y. Liu, W. Jin and X. Chen, *Biosens. Bioelectron.*, 2014, **54**, 165–170.
37 S. J. Gregg, K. S. W. Sing and H. W. Salzberg, *J. Electrochem. Soc.*, 1967, **114**, 279C.
38 Y. H. Tan, J. A. Davis, K. Fujikawa, N. V. Ganesh, A. V. Demchenko and K. J. Stin, *J. Mater. Chem.*, 2012, **22**, 6733–6745.
39 J. Zhang, S. Song, L. Wang, D. Pan and C. Fan, *Nat. Protoc.*, 2007, **2**, 2888–2895.
40 S. Guo, L. Wang and E. Wang, *Chem. Commun.*, 2007, 3163–3165.
41 F. Xu, K. Cui, Y. Sun, C. Guo, Z. Liu, Y. Zhang, Y. Shi and Z. Li, *Talanta*, 2010, **82**, 1845–1852.
42 F. Lisdat and D. Schaefer, *Anal. Bioanal. Chem.*, 2008, **391**, 1555–1567.
43 J. Chen, J. Zhang, J. Li, F. Fu, H. H. Yang and G. Chen, *Chem. Commun.*, 2010, **46**, 5939–5941.
44 Z. G. Yu and R. Y. Lai, *Chem. Commun.*, 2012, **48**, 10523–10525.
45 A. B. Steel, T. M. Herne and M. J. Tarlov, *Anal. Chem.*, 1998, **70**, 4670–4677.
46 J. Zhang, S. Song, L. Zhang, L. Wang, H. Wu, D. Pan and C. Fan, *J. Am. Chem. Soc.*, 2006, **128**, 8575–8580.
47 L. Li, H. Zhao, Z. Chen, X. Mu and L. Guo, *Biosens. Bioelectron.*, 2011, **30**, 261–266.
48 Y. Xiao, A. A. Lubin, A. J. Heeger and K. W. Plaxco, *Angew. Chem., Int. Ed.*, 2005, **44**, 5456–5459.
49 H. Y. Bai, F. Javier Del Campo and Y. C. Tsai, *Biosens. Bioelectron.*, 2013, **42**, 17–22.
50 H. Fan, H. Li, Q. Wang, P. He and Y. Fang, *Biosens. Bioelectron.*, 2012, **35**, 33–36.